HHS Public Access

Author manuscript

Nat Immunol. Author manuscript; available in PMC 2018 January 31.

Published in final edited form as:

Nat Immunol. 2016 October ; 17(10): 1159–1166. doi:10.1038/ni.3523.

CD1a on Langerhans cells controls inflammatory skin diseases

Ji Hyung Kim[#1], **Yu Hu**[#1], **Tang Yongqing**[2,3], **Jessica Kim**[1], **Victoria A. Hughes**[2,3], **Jérôme Le Nours**[2,3], **Elsa A. Marquez**[2,3], **Anthony W. Purcell**[2], **Qi Wan**[1], **Masahiko Sugita**[4], **Jamie Rossjohn**[#2,3,5,*], and **Florian Winau**[#1,*]

[1] Program in Cellular and Molecular Medicine, Boston Children's Hospital, Department of Microbiology and Immunobiology, Harvard Medical School, Boston, MA, USA

[2] Infection and Immunity Program & Department of Biochemistry and Molecular Biology, Biomedicine Discovery Institute, Monash University, Clayton, Victoria, Australia

[3] Australian Research Council Centre of Excellence in Advanced Molecular Imaging, Monash University, Clayton, Victoria, Australia

[4] Laboratory of Cell Regulation, Institute for Virus Research, Kyoto University, Kyoto, Japan

[5] Institute of Infection and Immunity, Cardiff University, School of Medicine, Heath Park, Cardiff, UK

[#] These authors contributed equally to this work.

Abstract

CD1a is a lipid-presenting molecule abundantly expressed on Langerhans cells. However, the *in vivo* role of CD1a remains unclear, principally because CD1a is lacking in mice. Using CD1a-transgenic mice, we show that the plant-derived lipid urushiol triggers CD1a-dependent skin inflammation, driven by $CD4^+$ T cells producing IL-17 and IL-22. Human subjects with poison ivy dermatitis showed a similar cytokine signature following CD1a-mediated urushiol recognition. Among different urushiol congeners, we identified diunsaturated pentadecylcatechol (C15:2) as the dominant antigen for CD1a-restricted T cells. We determined the crystal structure of the CD1a-urushiol (C15:2) complex, demonstrating the molecular basis of urushiol interaction with the antigen-binding cleft of CD1a. In a mouse model and psoriasis patients, CD1a amplified inflammatory responses mediated by T_H17 cells reactive with self lipid antigens. Treatment with blocking antibodies against CD1a alleviated skin inflammation. Thus, we propose CD1a as a potential therapeutic target in inflammatory skin diseases.

[*]Correspondence to: jamie.rossjohn@monash.edu, or florian.winau@childrens.harvard.edu.

AUTHOR CONTRIBUTIONS

J.H.K. and Y.H. designed and performed experiments, and wrote the manuscript. T.Y. performed crystallography and structural analysis. Q.W. and J.K. performed flow cytometry and helped revise the manuscript. V.A.H., J.L.N., E.A.M., and A.W.P. performed HPLC, mass spectrometry, crystallography, and analyzed data. M.S. generated human CD1a-transgenic mice. J.R. and F.W. designed and supervised experiments, and wrote the manuscript.

Supplementary Information is available in the online version of the paper.

Accession codes. Protein Data Bank: CD1a-urushiol, 5J1A; BK6 TCR–CD1a–endo, 4X6D.

COMPETING FINANCIAL INTERESTS

The authors declare no competing financial interest.

The family of CD1 molecules consists of group 1 CD1 (CD1a, b, c, and e) and group 2 CD1 (CD1d) proteins[1]. In contrast to MHC proteins that present peptides, CD1 molecules present lipid antigens to T lymphocytes[1,2]. For example, the CD1d molecule presents α-anomeric glycosphingolipids to invariant NKT cells[3], whereas CD1a-c molecules are mainly described to present lipids and lipopeptides from mycobacteria to a diverse T cell repertoire[4]. Notably, CD1a can display a broad spectrum of exogenous lipid antigens derived from pollen[5] or bacteria[6-8]. In addition, CD1a also presents self lipid antigens from host origin[9-15], such as triacylglycerol, squalene, wax ester, and fatty acid, which are enriched in the skin epidermis[11].

The abundant expression of CD1a hallmarks Langerhans cells in the skin. Langerhans cells (LCs) originate from yolk-sac-derived fetal liver progenitors[16,17], require IL-34 for development[18,19], and constitute the principal dendritic cell (DC) subset in the epidermis[20,21]. Additionally, the dermis harbors dermal as well as langerin-positive DCs. The three DC types in the skin fulfill different functions in antigen presentation: Langerin-positive dermal DCs are important for cross-priming of CD8 T cells, whereas Langerhans cells preferentially induce T_H17 cells[22,23].

The intricate immune system of the skin is critically involved in responses to extrinsic insults like allergens[24], as well as in autoimmune diseases, such as psoriasis[25,26]. Contact dermatitis is a common skin disease caused by exposure to small organic or inorganic molecules[24]. During the sensitization phase, allergen-specific T lymphocytes are generated that mediate skin inflammation upon challenge with the same antigen[24]. The sap compound urushiol found in the plants of the *Toxicodendron genus*, such as poison oak, poison sumac, and especially poison ivy[27], can trigger severe inflammation, and urushiol-specific T cells have been implicated in this process in the human system[28-30]. Psoriasis is a chronically relapsing, T cell-mediated inflammatory skin disease with a prevalence of 2-3% worldwide[25,26]. The disease is characterized by epidermal thickening (acanthosis), which leads to itchy and scaling macroscopic plaques[25,26]. It is well known that the cytokines IL-17 and IL-22 are crucial for the development of psoriasis[26]. Although psoriasis is considered an autoimmune disease, the identity of the antigens recognized remain elusive[26].

Considering that Langerhans cells predominantly express CD1a and reside in the epidermis that is readily accessible to foreign as well as self-lipid antigens, Langerhans cells and CD1a-restricted T cells are prime candidates for regulating skin immunity. However, since CD1a is expressed in humans but lacking in mice[1], the *in vivo* functions of CD1a on Langerhans have not been addressed and remain unclear.

Here, we show the vital importance of Langerhans cells expressing CD1a in skin inflammation *in vivo*. To demonstrate a role of CD1a on Langerhans cells in the induction of inflamma tory skin diseases, we used human CD1a-transgenic mice and found that CD1a drives pathogenesis of poison ivy dermatitis and psoriasis. Furthermore, we showed that CD1a-mediated skin inflammation is abrogated by CD1a blocking antibodies, highlighting CD1a as a novel target for treatment of inflammatory skin diseases.

RESULTS

CD1a promotes skin inflammation in response to poison ivy

CD1a presents lipid antigens with defined alkyl chain length to activate T cells[9,11,15]. Based on its lipophilic nature and size, we hypothesized that urushiol could represent a ligand displayed by CD1a to cause inflammation. To this end, we sensitized and challenged CD1a-transgenic (CD1a-tg) or wild-type mice with urushiol applied to the ear skin. Ear thickness as a first indicator of inflammation was strikingly increased in the presence of CD1a (**Fig. 1a**). Histological analysis revealed a pronounced cellular infiltrate especially in the dermis of urushiol-treated CD1a-tg animals (**Fig. 1b**). We analyzed the skin-infiltrating cells by flow cytometry and found a significant increase in inflammatory granulocytes and macrophages in CD1a-tg mice (**Fig. 1c,d**). Dermal T lymphocytes bearing a γδ T cell receptor (TCR) proliferated to the same extent in both mouse strains (**Fig. 1e,f**). By contrast, the presence of CD1a promoted the specific amplification of CD4 αβ T cells numbers, whereas the participation of CD8 T cells proved to be negligible (**Fig. 1e,f**). Investigating the functional cytokine responses of these lymphocytes, we found that the abundance of CD4 T cells producing IL-17 and IL-22 (T_H17 cells) was drastically increased in the CD1a-tg mouse model (**Fig. 1g,h**). Thus, CD1a promotes T_H17-mediated skin inflammation in response to poison ivy-derived urushiol. Next, we investigated whether our findings in the mouse model were relevant in humans. For this purpose, we tested $CD45RO^+$ memory T cells from the blood of human subjects (n = 6) who experienced moderate-to-severe poison ivy rash in the past six months. CD1a-transfectant antigen-presenting cells (K562 cell) or parental control cells were pulsed with urushiol or vehicle, prior to coculture with T lymphocytes from poison ivy or healthy donors. Subsequent analysis of T cell activation revealed increased IL-17- and IL-22 production of T cells from poison ivy donors that specifically responded to urushiol in a CD1a-dependent manner (**Fig. 2a,b**). Thus, in the context of our data in the CD1atransgenic system, human subjects with poison ivy dermatitis showed a similar inflammatory cytokine signature following CD1a-mediated urushiol recognition.

Adaptive immunity to urushiol differs from a hapten response

Next, we determined whether the immune response to urushiol was based on adaptive immunity, or innate mechanisms locally at work in the skin. In the absence of initial sensitization, CD1a-tg mice that were only challenged with urushiol failed to develop increased skin inflammation, as indicated by skin infiltration and IL-17-producing CD4 T cells (**Fig 3a,b**). Although urushiol showed a direct impact on innate inflammation, upregulation of inflammatory mediators, such as IL-1β and TNF, was comparable between CD1a-tg and wild-type mice (**Supplementary Fig. 1**). Therefore, CD1a-dependent immunity to urushiol involves antigen-specific T cell priming. To exclude a generally increased susceptibility of CD1a-tg mice to antigenic stimulation, we tested the immune response to the classical hapten dinitrofluorobenzene (DNFB)[24]. Surprisingly, ear swelling was reduced in the CD1a-tg mouse model when compared to wild-type (**Supplementary Fig. 2a**). In addition to reduced influx of inflammatory granulocytes, CD1a-tg mice generated drastically less CD8 T cells in response to DNFB and accordingly showed reduced IFN-γ production (**Supplementary Fig. 2b,c**). Thus, the CD1a-tg mice do not have a generally increased susceptibility to stimulation with hapten.

CD1a on LCs is important for T_H17-mediated dermatitis

Using confocal microscopy of epidermal sheets, we demonstrated the Langerhans cell network in the epidermis as well as their exclusive CD1a expression in the CD1a-tg mouse model (**Fig. 4a**). Moreover, we analyzed all skin DCs by flow cytometry and found the CD1a-positive population to superimpose with langerin-expressing Langerhans cells (**Fig. 4b**). Subsequently, we monitored CD1a expression on skin DCs during the immune response to urushiol. In vehicle-treated control skin, the composition of skin DCs proved to be comparable between CD1a-tg and wild-type mice, indicating normal homeostasis (**Fig. 4c**). In the inflamed ear skin, we observed a massive influx of inflammatory, CD1a-negative DCs. By contrast, epidermal Langerhans cells were the main population specifically expressing CD1a in poison ivy dermatitis (**Fig. 4c**). Based on this exclusive expression pattern, we next aimed at inhibiting CD1a function on Langerhans cells. For this purpose, we treated mice during the sensitization phase with CD1a blocking antibodies. Strikingly, anti-CD1a treatment reduced ear swelling in CD1a-tg animals to wild-type levels as compared to administration of isotype control antibodies (**Fig. 4d**). Accordingly, infiltration of inflammatory granulocytes and IL-17-producing CD4 T cells was equally abrogated by anti-CD1a treatment (**Fig. 4e,f**). Of note, antibody application had no depletional effect but rather blocked CD1a function on the surface of Langerhans cells. In this context, we found downregulation of CD1a on skin Langerhans cells upon antibody treatment, although diminishment of CD1a appeared incomplete possibly due to limited accessibility of the epidermis for systemically administered antibodies **(Fig. 4g**). However, in skin-draining lymph nodes, anti-CD1a treatment led to full downregulation of CD1a on migrating Langerhans cells (**Fig. 4g**). Taken together, CD1a-expressing Langerhans cells are essential for generation of T_H17 cells and skin inflammation.

Urushiol (C15:2) is an antigen for CD1a-restricted T cells

Since poison ivy induced strong CD1a-mediated inflammation, we next investigated whether urushiol is a bona fide antigen presented by CD1a. For this purpose, we incubated plate-bound recombinant human CD1a molecules with urushiol, prior to culture with CD4 T cells isolated from urushiol-immunized mice. In sharp contrast to lymphocytes from wild-type mice, only CD4 T cells isolated from CD1a-tg animals produced IL-17 in response to urushiol-loaded CD1a molecules (**Fig. 5a**). This system is free of antigen-presenting cells and thus demonstrates the direct presentation of urushiol by CD1a. Since natural urushiol contains a mixture of different pentadecylcatechols, we subsequently determined which congener of poison ivy was responsible for its antigenic properties. Using the same recombinant CD1a system and synthetically generated urushiol congeners, we found that pentadecylcatechol with two unsaturations (C15:2) is the dominant immunogen for CD1a-mediated T cell activation (**Fig. 5b**). We also showed that C15:2 mediated the observed effects of increased skin inflammation in CD1a-tg mice (**Fig. 5c**). In order to mimic urushiol presentation in its natural habitat, we isolated Langerhans cells from ear skin of immunized CD1a-tg animals, prior to pulsing with C15:2 and coculture with CD4 T cells from draining lymph nodes. Langerhans cells triggered a strong T_H17 cell response upon C15:2 presentation in a strictly CD1a-specific manner, because anti-CD1a fully abolished T cell activation (**Fig. 5d**). Of note, a substantial degree of autoreactive, CD1a-restricted T cell

stimulation could be observed with unpulsed Langerhans cells (**Fig. 5d**). A classical feature of adaptive immunity is the clonal expansion of antigen-specific T cells, characterized by a certain TCR usage of amplified cells. Therefore, we investigated the TCR repertoire of the immune response to urushiol. Notably, T cells exhibited a significant increase in Vβ2 and Vβ4 TCR usage in inflamed skin of CD1a-tg mice, suggesting clonal expansion under antigenic selection pressure (**Supplementary Fig. 3a**). The $V\beta2^+$ and $V\beta4^+$ T cell clones produced higher amounts of IL-17 in CD1a-tg animals compared to wild-type mice (**Supplementary Fig. 3b**). Moreover, amplification of $V\beta2^+$ and $V\beta4^+$ T cells was significantly hampered when CD1a function was blocked by antibody treatment (**Supplementary Fig. 3c**). These changes in TCR repertoire were specific for T cells in skin inflammation, because normal control skin showed no difference in TCR usage between wild-type and CD1a-tg mice (**Supplementary Fig. 3d**). Additionally, the CD1a-tg mouse model revealed no alterations of the TCR repertoire in the thymus, excluding differential thymic selection (**Supplementary Fig. 3e**). Altogether, our results on functional presentation and TCR repertoire suggest that urushiol is an antigen for CD1a-restricted T cells.

Crystal structure of the CD1a-urushiol (C15:2) complex

Therefore, we aimed to obtain molecular insight into the mechanism of CD1a presenting urushiol. To establish this, we recombinantly expressed the CD1a molecule in mammalian cells and *in vitro* loaded the urushiol ligand (C15:2). As CD1a expressed in mammalian cells presents an heterogeneous array of self lipid ligands within its antigen-binding cleft, the endogenous lipids were initially displaced by the ganglioside GD_3. Subsequently, GD_3 bound to CD1a was specifically displaced by urushiol, with the CD1a-urushiol complex being purified from CD1a-GD_3 via anion-exchange chromatography. Next, we crystallized and determined the structure of the CD1a-urushiol binary complex to 1.9Å resolution (**Fig. 6a** and **Supplementary Table 1**). Unbiased electron density was visible for the urushiol ligand, with the ligand clearly being non-covalently bound within the CD1a antigen-binding cleft (**Supplementary Fig. 4a,b**). Mass spectrometry analysis confirmed the presence of urushiol (m/z 317.24) both in the purified recombinant CD1a sample loaded with urushiol and in crystals of the CD1a-urushiol binary complex (**Fig. 6b,c**). Accordingly, CD1a directly presents urushiol.

The antigen-binding cleft of CD1a comprises the A′- and F′-pockets, in which the A′-pocket is considered to function as a molecular ruler, favoring acyl chains between C_{18}-$_{23}$ in length[15]. For example, in the structure of the CD1a-lysophosphatidylcholine complex, the acyl chain winds round the A′-pocket while the polar headgroup is positioned at the junction of A′- and F′-portals[9]. As anticipated, the urushiol antigen is positioned deep in the CD1a binding cleft, spanning from the A′- to the F′-pocket (**Fig. 7a**). Surprisingly however, the catechol headgroup and acyl chain were positioned towards the A′- and F′-pockets, respectively, in the reverse direction to what may have been anticipated based on previous CD1a-antigen structures (**Fig. 6a**, right panel)[5]. Here, the urushiol antigen mainly interacted via van der Waals contacts with residues of the α1-helix of CD1a (**Fig. 6a** and **Supplementary Table 2**). The aromatic catechol headgroup of the antigen was positioned in the A'-pocket and stacked against Phe70, while the 3′-hydroxyl formed a hydrogen bond

with the main chain carbonyl of Leu66. The C15:2 aliphatic tail of urushiol sat over the hydrophobic platform formed by Val12, Trp14, Val98, and Leu116 (**Fig. 6a**). 80% of the urushiol molecule is buried within the CD1a cleft (Buried Surface Area of ~495 $Å^2$). Thus, CD1a presents the urushiol antigen with 20% of its molecular surface potentially exposed at the F'-portal for direct TCR contact (**Fig. 7b**).

CD1a facilitates T_H17-driven psoriatic skin inflammation

Based on the substantial IL-17 production by CD1a-autoreactive T cells (**Fig. 5d**) and the prominent function of IL-17 in psoriasis[25,26], we hypothesized that CD1a might play an important role in psoriatic inflammation. Therefore, we investigated CD1a-tg mice in a well-established model for psoriasiform inflammation, using skin administration of the small molecule compound imiquimod[31]. Histological analysis revealed strong cellular infiltration of the skin and dramatic epidermal hyperplasia in CD1a-tg mice when compared to controls (**Fig. 8a**). Histopathology was reflected in the macroscopic, psoriasis-like aspect of ear skin that exhibited swelling, reddening, and scaling (**Fig. 8a,b**). Next, we aimed at therapy of psoriasiform inflammation using CD1a blocking antibodies. Anti-CD1a treatment significantly reduced skin inflammation in CD1a-tg animals (**Fig. 8c**). This therapeutic effect was mirrored by reduction of inflammatory granulocytes and CD4 T cells that produced IL-17A, IL-17F, and IL-22 (**Fig. 8d,e**). Taking into account that we did not challenge CD1a-tg mice with exogenous lipids in this psoriasis model, we hypothesized that during the inflammatory process, self lipid antigens are released to facilitate CD1a-mediated T cell responses and skin inflammation. To this end, we isolated T cells from skin-draining lymph nodes of imiquimod-treated mice, prior to incubation with plate-bound CD1a molecules loaded with self lipids that have been previously reported as skin antigens[11]. T cells from CD1a-tg mice specifically responded to CD1a-restricted self lipid presentation, with pronounced recognition of fatty acid, squalene, wax ester, and triacylglycerol (**Fig. 8f**). Of note, we could not detect any meaningful production of IL-17 in untreated controls, underscoring that in the absence of inflammation, there is a complete lack of self lipid antigen presentation and recognition (**Fig. 8f**). Ultimately, we wanted to translate our findings in the psoriasis-like model to the human system. For this purpose, we studied a cohort of patients with moderate-to-severe plaque psoriasis compared to healthy donors, measuring CD1a-restricted T cell activation. Accordingly, $CD45RO^+$ memory T cells from the blood of psoriasis patients (n = 6) or healthy donors (n = 6) were stimulated with autologous monocyte-derived DCs in the presence or absence of anti-CD1a, prior to measurement of cytokine responses. Notably, we observed an increase in protein production of IL-17 and IL-22 in T cells from psoriasis patients when compared to healthy controls (**Fig. 8g**). Moreover, the inflammatory cytokine response from patients was significantly blocked by anti-CD1a treatment (**Fig. 8g**). Taking the mouse model for psoriasis and human studies together, we present strong evidence that CD1a drives psoriatic skin inflammation and that targeting CD1a can abrogate inflammatory skin disease.

DISCUSSION

Using human CD1a-transgenic mice, our studies demonstrate a vital role for CD1a in skin inflammation *in vivo*. Since wild-type mice lack CD1a expression, previous reports

investigating Langerhans cell functions in the murine system neglect the integral role of CD1a in humans. Therefore, the CD1a-tg mouse model is able to demonstrate the entire spectrum of Langerhans cell abilities, including CD1a as their prominent hallmark molecule. We show that poison ivy-induced skin inflammation is dominated by CD1a-dependent T_H17 cells. Using wild-type mice in the absence of CD1a, previous work suggested CD8 T cells and IFN-γ to respond to urushiol[32]. However, the magnitude of inflammation appeared to be relatively mild[32], which is in agreement with our observations in control animals. In sharp contrast, the response to poison ivy is much stronger in humans, including skin reddening, blistering, and vigorous itch – a severity well reflected in the CD1a-transgenic mouse model. Urushiol is commonly considered a prohapten, whose catechol group is oxidized to a quinone that subsequently reacts with endogenous proteins to form an immunogen[24]. Normally, contact hypersensitivity to haptens is driven by CD8 T cells producing IFN-γ, as seen in response to DNFB and drug hypersensitivities[24,33]. By contrast, we demonstrate urushiol-specific, CD1a-restricted activation of CD4 T cells that secrete IL-17. Moreover, immune stimulation by DNFB was suppressed in CD1a-tg mice. As Langerhans cells are important in suppression of hapten responses[22,24], CD1a-expressing Langerhans cells may be implicated in dampened DNFB responses.

Based on presentation experiments using recombinant CD1a or Langerhans cells, and our structural studies on the CD1a-urushiol complex, we demonstrate that urushiol (C15:2) is a *de facto* antigen for CD1a-restricted T cells. While the overall structural features of the CD1a binding cleft were generally conserved upon urushiol binding by comparison to the previous CD1a-antigen complexes[9], two CD1a residues deep within the A′-pocket underwent structural rearrangements in order to accommodate the urushiol antigen in the binding groove. Namely, Phe70 and Trp14 swung away to provide space for the catechol headgroup and the C15-tail of urushiol, respectively. These conformational changes had the knock-on effect of altering the conformation of the CD1a antigen-binding cleft (root mean square deviation of 0.6 Å), in particular residues 146-150 (r.m.s.d. of 1.3 Å), which subsequently impacted on the conformation of Arg73, Arg76, and Glu154, a constellation of residues known to impact on the autoreactivity of a CD1a-restricted TCR[9]. Thus, a region of the urushiol antigen is accessible for direct TCR contact within the CD1a groove, and moreover, the accommodation of urushiol leads to conformational changes within CD1a that could also directly impact on TCR recognition. However, future studies will be required to show the ternary structure of CD1a-urushiol-TCR.

Furthermore, we demonstrated that CD1a on Langerhans cells controls inflammation in psoriasis, exploring a psoriasis-like mouse model as well as patients. Considering our findings on presentation of fatty acid and triacylglycerol, we propose that self lipids could represent dominant antigens in psoriasis when displayed by CD1a. A study revealed that self lipids fitting into the CD1a binding groove can change the conformation of CD1a to be recognized by specific TCRs, in a mechanism of permissive autoreactivity[9]. Integrating follow-up human studies using patient samples, the concept of self lipids might provide important answers to the long quest for antigens so far unknown in psoriasis. The skin harbors a multitude of immune cells involved in the response to challenges. Dermal γδ T cells produce IL-17 and have been associated with psoriasis[34,35]. We observed a comparable increase of dermal γδ T cells in CD1a-tg or wild-type mice in response to urushiol or

imiquimod. By contrast, amplification of IL-17-producing αβ T cells was specific for the CD1a-tg model, thus explaining the predominant impact of CD1a-dependent T_H17 cells on skin inflammation. Yet, both T cell populations can complement each other, with γδ T cells responding early and in an innate fashion to cytokines such as IL-23, and CD1a-restricted T_H17 cells acting at a later stage in a lipid antigen-specific manner. In psoriasis patients, we found a particular increase in inflammatory IL-17 and IL-22 production upon recognition of CD1a. Finally, our results demonstrate that blocking CD1a *in vivo* using antibody treatment is able to substantially reduce skin inflammation. Thus, we propose targeting of CD1a to pave the way for future CD1a-based therapies against inflammatory skin diseases.

METHODS

Reagents

RPMI medium 1640, propidium iodide (PI), ethylenediaminetetraacetic acid (EDTA), β-mercaptoethanol, penicillin and streptomycin, sodium pyruvate, and L-glutamine were purchased from Life Technologies. Fetal bovine serum (FBS), bovine serum albumin (BSA), and phosphate-buffered saline (PBS) were from Sigma-Aldrich. RPMI medium 1640 was supplemented with 10% FBS, penicillin and streptomycin (10 U/ml), sodium pyruvate (1 mM), L-glutamine (2 mM), β-mercaptoethanol (50 μM), and HEPES (100 mM). Purified natural urushiol was a generous gift from Alfred Del Grosso at the Food and Drug Administration (FDA). Synthetic urushiols C15:1, C15:2, and C15:3 were purchased from Phytolab (Germany). Synthetic urushiol C15:0 was obtained from ChromaDex. Palmitoleic acid, squalene, and glyceryl tripalmitoleate were purchased from Sigma-Aldrich. Oleyl palmitoleate and oleyl oleate were from Nu-Chek.

Antibodies

For flow cytometry, cells were stained using antibodies and dilutions in **Supplementary Table 3**. Anti-CD1a antibody (10H3) for blocking was kindly provided by M. Brenner. Secondary antibodies anti-mouse IgG (cat. no.: A-11001, Life Technologies) and anti-rat IgG (cat. no.: A-21434, Life Technologies) were from Life Technologies. To study the repertoire of Vβ TCRs, the Mouse Vβ TCR Screening Panel (cat. no.: 557004, BD Pharmingen) was used.

Mice and models of skin inflammation

Human CD1a-transgenic mice (CD1a-tg) were generated as previously reported[36]. Briefly, a fragment of the human genomic *CD1a* was introduced into mouse. CD1a was exclusively found on immature thymocytes and Langerhans cells, similar to the expression pattern of CD1a in human. C57/BL6/J and OT-II transgenic mice were purchased from The Jackson Laboratory. Sex- and age-matched animals between 8 and 12 weeks of age were used for experiments. Preliminary experiments were performed to determine proper sample size. All animal experiments were approved by the Institutional Animal Care and Use Committee (IACUC) of Harvard Medical School. For triggering skin inflammation, mice were sensitized on the shaved abdomen with 30 μl of 20 mg/ml urushiol, or 0.5% DNFB (Sigma) dissolved in acetone (Sigma). Five days after sensitization, mice were challenged on dorsal and ventral side of the ear with 10 μl of 5 mg/ml urushiol or 0.2% DNFB. To induce

psoriatic skin inflammation, 5% imiquimod cream (Glenmark) was topically applied on dorsal and ventral sides of ears for 6-7 consecutive days as previously described[37]. Ear thickness was measured before and after treatment using a micrometer (Swiss Precision Instruments). To block CD1a-dependent responses, mice were injected with 100 μg of anti-CD1a or isotype control antibody at −3, −1, +1, +3, +5 days before and after treatment.

Mouse tissue preparation

Ears were excised, split into two halves at an angle parallel to the cartilage, and further cut into small pieces. Tissue samples were digested in RPMI containing 0.1 mg/ml Liberase TM (Roche Diagnostic Corp.), 0.1 mg/ml DNase I (Roche Diagnostic Corp.), and 20 μM HEPES (Life Technologies) for 2 hours at 37°C with shaking (140 rpm). Digested samples were minced through a metal mesh, and filtered with a 70 μm nylon strainer (BD Biosciences). Auricular lymph nodes and thymi were harvested and minced through a metal mesh to obtain single cell suspensions. To isolate CD4 T cells, cell suspensions were incubated with anti-CD16/CD32 for 10 minutes on ice, and CD4-positive cells were selected using CD4 magnetic beads and MACS columns (Miltenyi Biotec) according to manufacturer's protocol.

Langerhans cell isolation

Langerhans cells (LCs) from ear skin were isolated as previously described[38]. Briefly, ears were split into dorsal and ventral halves, and incubated in 0.8% trypsin solution (Sigma-Aldrich) for 25-45 minutes at 37°C. Epidermal layers were peeled off from the dermis and transferred into complete RPMI medium, followed by stirring for 40 minutes at 37°C in a water bath incubator (Labline Instruments). Cell suspensions were passed through 70 μm nylon strainers. To remove dead cells, a gradient centrifugation with Percoll (GE Healthcare) was performed. Cells were stained with anti-CD11c magnetic beads, and CD11c-positive cells were sorted by MACS columns. Approximately 70% of isolated cells were $CD1a^{+}MHCII^{+}$ LCs.

T cell assay with LCs

LCs were pulsed with 5 μg/ml urushiol or vehicle in complete media for 2 hours, and subsequently co-cultured with T cells at a ratio of 1:5 in 96-well round-bottom plates. To block CD1a-dependent responses, LCs were incubated with 10 μg/ml anti-CD1a (10H3) or isotype control antibody for 2 hours, prior to the addition of T cells. After 3 days, culture supernatants were harvested to perform ELISA for IL-17A and IFN-γ.

T cell experiments with plate-bound recombinant CD1a

Biotinylated CD1a monomers paired with β_2-microglobulin were provided by the NIH Tetramer Facility. CD1a-coated plates and lipid antigens were prepared as described previously[11]. Briefly, streptavidin-coated plates (Thermo Scientific) were incubated with biotinylated human CD1a-β_2-microglobulin monomers (1 μg/well) and anti-CD11a (0.25 μg/ml) in PBS for 18 hours at room temperature. After washing with PBS, the plates were incubated with citrate buffer (pH 3.4) for 20 minutes, repeated twice with three washing steps in between. Lipid antigens were dissolved in PBS containing 0.05% Tween 20 (1-100 μM) by sonication for 30 minutes at room temperature in a water bath sonicator (Branson),

followed by heating at 56°C for 20 minutes, prior to addition to plates coated with CD1a. After 48 hours of incubation at room temperature, the plates were washed with PBS three times. T cells suspended in complete media were added to the plates ($1\text{-}2\times10^4$ skin CD4 T cells, or 1×10^5 lymph node CD4 T cells per well), and cultured for 3-5 days at 37°C in a CO_2 incubator (Thermo Scientific). Culture supernatants were used for cytokine analysis by ELISA.

Human T cell assays

For the psoriasis study, patients diagnosed with moderate-to-severe plaque psoriasis were included in the study based on their Psoriasis Area Severity Index (PASI). The PASI integrates criteria including erythema, induration, desquamation, and percentage of affected skin area. Monocyte-derived CD1a-expressing dendritic cells (mDCs) and $CD45RO^+$ memory CD4 T cells were prepared as previously described[12]. mDCs were treated with LPS (100 ng/ml) for 3 hours, prior to coculture with CD4 T cells. After expansion for 10 days, T cells were tested for CD1a auto-reactivity by co-culture with autologous mDCs at a ratio of 1:5 for 3 days in the presence of 10 μg/ml anti-CD1a or isotype control. To test urushiol-specific T cell responses in humans, $CD45RO^+$ memory T cells isolated from peripheral blood mononuclear cells (PBMCs) of subjects who had poison ivy dermatitis in the last 6 months or control donors were expanded with autologous DCs pulsed with 2 μg/ml urushiol C15:2 for 10 days. Human IL-2 was added every 3 days during cell culture. Subsequently, urushiol-specific T cell responses were determined by co-culture of expanded T cells with urushiol C15:2- or vehicle-pulsed CD1a- or mock-transfected K562 cells at a ratio of 1:5. Three days after co-incubation, cells were used for intracellular cytokine staining and analyzed by flow cytometry, and culture supernatants were used for cytokine analysis by ELISA. K562 cells were routinely tested for mycoplasma contamination, and CD1a expression of transfectants was confirmed before use by flow cytometry. PBMCs were obtained from ConversantBio, ALLCELLS, and the Kraft Family Blood Donor Center at Brigham and Women's Hospital. Informed consent was obtained from all subjects, and all human studies were approved by Boston Children's Hospital's Institutional Review Board (IRB).

Flow cytometry and intracellular staining for cytokines

Cells were stained with antibodies against surface antigens in FACS buffer (PBS supplemented with 0.5% BSA) on ice for 30 minutes. Subsequently, cells were washed and analyzed using a FACSCanto™ II flow cytometer (BD Biosciences). Propidium iodide or viability dye (eBioscience) was used to exclude dead cells. For intracellular cytokine staining, cells were stimulated *ex vivo* with 50 ng/ml phorbol myristate acetate (Sigma), and 5 μg/ml ionomycin (Sigma) in the presence of brefeldin A (BioLegend) in complete media for 4 hours at 37°C in a CO_2 incubator. After surface staining, cells were fixed and permeabilized with BD Cytofix/Cytoperm solution followed by staining with antibodies against cytokines in Perm/Wash buffer (BD Biosciences).

RNA extraction and real-time qPCR

Total RNA was purified from ear cells using the RNeasy Plus Mini Kit (Qiagen) according to the manufacturer's instructions. RNA was converted to cDNA with High Capacity *RNA*-

to-*cDNA* Kit (Applied Biosystems). cDNA was mixed with primers and iTaq universal *SYBR Green* supermix (Bio-Rad), and relative expression was determined by real-time PCR using a 7300 Real-Time PCR System (Applied Biosystems). β-actin was used as a housekeeping control. To calculate the relative fold change, the $2^{-\Delta\Delta CT}$ cycle threshold method was used. The primer sequences are described in **Supplementary Table 4**.

Histology and confocal microscopy

Mice were euthanized by CO_2 inhalation, and ear samples were frozen in Optimal Cutting Temperature (OCT) compound (Sakura Finetechnical Corporation). Ten μm-thick cross-sections were made and stained with hematoxylin and eosin by the Histology Core at Beth Israel Deaconess Medical Center. Images were taken using a BX63 Motorized Microscope (Olympus). For epidermal sheets, ear pinnae were treated with shaving cream (SoftSheen-Carson) and affixed to slides with the epidermis downward. The ear samples were incubated in 10 mM EDTA in PBS for 2 hours at 37°C, followed by physical removal of the dermis. Tissue was fixed in 4% paraformaldehyde (Sigma) at room temperature for 30 minutes, and blocked with 10% FBS and 2% goat serum (Life Technologies) in PBS. Tissues were stained with purified anti-MHC class II and anti-CD1a, followed by staining with Alexa Fluor 647-conjugated anti-rat IgG, and Alexa Fluor 488-conjugated anti-mouse IgG as secondary antibodies. Samples were mounted with ProLong® Gold Antifade Mountant including DAPI (Life Technologies). Immunofluorescent images were taken using an Olympus FV1000 confocal microscope.

Expression, purification of CD1a and urushiol (C15:2) loading into CD1a

The glycoprotein CD1a was expressed in a mammalian expression system and purified as previously described[9]. Following an endoglycosidase H (New England BioLabs) treatment, the purified CD1a was first loaded with the ganglioside GD_3 (GD_3) (Matreya LLC) that was dissolved in a solution containing 0.5% tyloxapol (Sigma) and 10 mM Tris buffer at pH 8.0. CD1a was first incubated with GD_3 overnight at room temperature at a molar ratio of 1:15. The CD1a sample loaded with GD_3 was further purified using ion exchange chromatography (MonoQ 10/100 GL-GE Healthcare). Urushiol C15:2 (Chemos) was dissolved in a solution containing 10 mM Tris buffer at pH 8.0 / 0.5% tyloxapol / 50% acetone (Sigma). The GD_3–CD1a sample was then incubated overnight with urushiol at a 1:15 molar ratio and at room temperature in order to achieve the GD_3 displacement by urushiol. A subsequent purification step involving ion exchange chromatography (MonoQ 10/100 GL) was performed to remove the excess of urushiol C15:2, GD_3 –CD1a, and detergent.

Crystallization, structure determination and refinement

Seeds obtained from previous binary CD1a-antigen crystals[9] were used to grow crystals of the CD1a-urushiol (C15:2) binary complex in 20-25% PEG 1500 / 10% MMT buffer pH 5-6. The crystals were flash-frozen and data were collected at the MX2 beamline (Australian Synchrotron) to a 1.9Å resolution. All the data were processed with the program MOSFLM and were scaled with the CCP4 suite[39]. Consistent with the mass spectrometry data, the urushiol antigen was clearly evident in the unbiased electron density maps, in addition a trace amount of an endogenous self antigen was also evident on account of the high

resolution of the binary complex. An initial run of rigid body refinement was performed with the refinement program BUSTER 2.10[40]. Iterative model improvement with COOT[41] and further refinement with BUSTER 2.10[40] were performed. The final refinement led to an R/R-free (%) of 18.6/21.6. The quality of the structure was confirmed at the Research Collaboratory for Structural Bioinformatics Protein Data Bank Data Validation and Deposition Services website. All presentations of molecular graphics were created with the PyMOL molecular visualization system (The PyMOL Molecular Graphics System, Version 1.5.0.4 Schrödinger, LLC.).

Extraction of urushiol and mass spectrometry analysis

In all samples, urushiol was extracted using a single phase Folch procedure[42] and analyzed using a Q-Exactive Hybrid Quadrupole-Orbitrap. Prior to urushiol extraction, crystals of CD1a-urushiol were extensively washed with the crystallization mother liquor and dissolved in Tris Buffer Saline (TBS), pH 8.0. MS coupled to a RSLC nano HPLC (Thermo Scientific, Bremen, Germany). Samples were loaded onto a nanoviper pepmap100 trap column (100μm × 2cm) in 2% acetonitrile / 0.1% ammonium acetate at a flow rate of 15 μL / minute. Analytes were separated at a flow rate of 300 μL / minute on a pepmap100 C18 column (75μm × 15cm, Thermo Scientific) using a linear gradient of acetonitrile (2-80%). Up to 12 MS/MS spectra were acquired per cycle with maximum accumulation time of 50 ms and 100 ms for MS1 and MS2, respectively. A SCIEX QTRAP 5500 mass spectrometer was used for MRM-based detection as previously described[43]. The 5500 mass spectrometer was operated with unit quadrupole resolution and three MRM transitions were simultaneously monitored in detecting U15 315.2→149.1, 315.2→135.1, 315.2→122.1. Data analysis was performed using a combination of Analyst v1.5.2 and XCalibar 3.0 (Thermo Fisher Scientific).

Statistical analysis

Data are presented as mean ± standard error. No statistical method was used to predetermine sample size, which instead was determined based on the results of preliminary experiments. Mice were allocated at random to experimental groups. Mouse studies were performed in a non-blinded fashion. To compare two groups, the two-tailed unpaired *t*-test, or Mann-Whitney, or Wilcoxon test was used with or without the assumption of normality, respectively. The variance between groups was similar within each group. To compare means between more than two groups, one-way or two-way ANOVA test was performed with post multiple comparisons. p values > 0.05 were considered not significant. All statistical analysis was calculated using Prism software (GraphPad).

Supplementary Material

Refer to Web version on PubMed Central for supplementary material.

ACKNOWLEDGENTS

We thank M. Brenner (Brigham and Women's Hospital, Boston) for providing CD1a antibody, B. Moody and T.-Y. Cheng (Brigham and Women's Hospital, Boston) for providing K562 cells and advice regarding human T cell assays. We are grateful to A. Del Grosso (Food and Drug Administration, Washington D.C.) for sharing natural urushiols. We thank U. von Andrian and J. Ordovas-Montanes (Harvard Medical School, Boston) for advice

regarding preparation of skin tissue. We thank the NIH tetramer facility for providing CD1a-monomers. We thank the staff at the Australian synchrotron for assistance with data collection. J.H.K. was supported by the National Research Foundation of Korea (2012R1A6A3A03040248) and the AMOREPACIFIC Research Scholar Program. J.R. was supported by an NHMRC Australia Fellowship. This work was supported by the NHMRC and the ARC (J.R.), and NIH grant R01 AI083426 (F.W.).

REFERENCES

1. Brigl M, Brenner MB. CD1: antigen presentation and T cell function. Annu. Rev. Immunol. 2004; 22:817–890. [PubMed: 15032598]
2. Porcelli S, et al. Recognition of cluster of differentiation 1 antigens by human CD4-CD8-cytolytic T lymphocytes. Nature. 1989; 341:447–450. [PubMed: 2477705]
3. Kain L, et al. The identification of the endogenous ligands of natural killer T cells reveals the presence of mammalian alpha-linked glycosylceramides. Immunity. 2014; 41:543–554. [PubMed: 25367571]
4. Van Rhijn I, Godfrey DI, Rossjohn J, Moody DB. Lipid and small-molecule display by CD1 and MR1. Nat. Rev. Immunol. 2015; 15:643–654. [PubMed: 26388332]
5. Agea E, et al. Human CD1-restricted T cell recognition of lipids from pollens. J. Exp. Med. 2005; 202:295–308. [PubMed: 16009719]
6. Hunger RE, et al. Langerhans cells utilize CD1a and langerin to efficiently present nonpeptide antigens to T cells. J. Clin. Invest. 2004; 113:701–708. [PubMed: 14991068]
7. Moody DB, et al. T cell activation by lipopeptide antigens. Science. 2004; 303:527–531. [PubMed: 14739458]
8. Pena-Cruz V, Ito S, Dascher CC, Brenner MB, Sugita M. Epidermal Langerhans cells efficiently mediate CD1a-dependent presentation of microbial lipid antigens to T cells. J. Invest. Dermatol. 2003; 121:517–521. [PubMed: 12925210]
9. Birkinshaw RW, et al. alphabeta T cell antigen receptor recognition of CD1a presenting self lipid ligands. Nat. Immunol. 2015; 16:258–266. [PubMed: 25642819]
10. Bourgeois EA, et al. Bee venom processes human skin lipids for presentation by CD1a. J. Exp. Med. 2015; 212:149–163. [PubMed: 25584012]
11. de Jong A, et al. CD1a-autoreactive T cells recognize natural skin oils that function as headless antigens. Nat. Immunol. 2014; 15:177–185. [PubMed: 24362891]
12. de Jong A, et al. CD1a-autoreactive T cells are a normal component of the human alphabeta T cell repertoire. Nat. Immunol. 2010; 11:1102–1109. [PubMed: 21037579]
13. de Lalla C, et al. High-frequency and adaptive-like dynamics of human CD1 self-reactive T cells. Eur. J. Immunol. 2011; 41:602–610. [PubMed: 21246542]
14. Jarrett R, et al. Filaggrin inhibits generation of CD1a neolipid antigens by house dust mite-derived phospholipase. Sci. Transl. Med. 2016; 8:325ra318.
15. Zajonc DM, Elsliger MA, Teyton L, Wilson IA. Crystal structure of CD1a in complex with a sulfatide self antigen at a resolution of 2.15 A. Nat. Immunol. 2003; 4:808–815. [PubMed: 12833155]
16. Gomez Perdiguero E, et al. Tissue-resident macrophages originate from yolk-sac-derived erythro-myeloid progenitors. Nature. 2015; 518:547–551. [PubMed: 25470051]
17. Hoeffel G, et al. Adult Langerhans cells derive predominantly from embryonic fetal liver monocytes with a minor contribution of yolk sac-derived macrophages. J. Exp. Med. 2012; 209:1167–1181. [PubMed: 22565823]
18. Greter M, et al. Stroma-derived interleukin-34 controls the development and maintenance of langerhans cells and the maintenance of microglia. Immunity. 2012; 37:1050–1060. [PubMed: 23177320]
19. Wang Y, et al. IL-34 is a tissue-restricted ligand of CSF1R required for the development of Langerhans cells and microglia. Nat. Immunol. 2012; 13:753–760. [PubMed: 22729249]
20. Igyarto BZ, Kaplan DH. Antigen presentation by Langerhans cells. Curr. Opin. Immunol. 2013; 25:115–119. [PubMed: 23246038]

21. Merad M, Ginhoux F, Collin M. Origin, homeostasis and function of Langerhans cells and other langerin-expressing dendritic cells. Nat. Rev. Immunol. 2008; 8:935–947. [PubMed: 19029989]
22. Bobr A, et al. Acute ablation of Langerhans cells enhances skin immune responses. J. Immunol. 2010; 185:4724–4728. [PubMed: 20855870]
23. Igyarto BZ, et al. Skin-resident murine dendritic cell subsets promote distinct and opposing antigen-specific T helper cell responses. Immunity. 2011; 35:260–272. [PubMed: 21782478]
24. Kaplan DH, Igyarto BZ, Gaspari AA. Early immune events in the induction of allergic contact dermatitis. Nat. Rev. Immunol. 2012; 12:114–124. [PubMed: 22240625]
25. Lowes MA, Bowcock AM, Krueger JG. Pathogenesis and therapy of psoriasis. Nature. 2007; 445:866–873. [PubMed: 17314973]
26. Perera GK, Di Meglio P, Nestle FO. Psoriasis. Annu. Rev. Pathol. 2012; 7:385–422. [PubMed: 22054142]
27. Walker SL, Lear JT, Beck MH. Toxicodendron dermatitis in the UK. Int. J. Dermatol. 2006; 45:810–813. [PubMed: 16863516]
28. Kalish RS. The use of human T-lymphocyte clones to study T-cell function in allergic contact dermatitis to urushiol. J. Invest. Dermatol. 1990; 94:108S–111S. [PubMed: 1693644]
29. Kalish RS, Johnson KL. Enrichment and function of urushiol (poison ivy)-specific T lymphocytes in lesions of allergic contact dermatitis to urushiol. J. Immunol. 1990; 145:3706–3713. [PubMed: 2147199]
30. Kalish RS, Wood JA, LaPorte A. Processing of urushiol (poison ivy) hapten by both endogenous and exogenous pathways for presentation to T cells in vitro. J. Clin. Invest. 1994; 93:2039–2047. [PubMed: 7910172]
31. van der Fits L, et al. Imiquimod-induced psoriasis-like skin inflammation in mice is mediated via the IL-23/IL-17 axis. J. Immunol. 2009; 182:5836–5845. [PubMed: 19380832]
32. Wakabayashi T, et al. IFN-gamma and TNF-alpha are involved in urushiol-induced contact hypersensitivity in mice. Immunol. Cell Biol. 2005; 83:18–24. [PubMed: 15661037]
33. Illing PT, et al. Immune self-reactivity triggered by drug-modified HLA-peptide repertoire. Nature. 2012; 486:554–558. [PubMed: 22722860]
34. Cai Y, et al. Pivotal role of dermal IL-17-producing gammadelta T cells in skin inflammation. Immunity. 2011; 35:596–610. [PubMed: 21982596]
35. Gray EE, Suzuki K, Cyster JG. Cutting edge: Identification of a motile IL-17-producing gammadelta T cell population in the dermis. J. Immunol. 2011; 186:6091–6095. [PubMed: 21536803]

References for Methods

36. Kobayashi C, et al. GM-CSF-independent CD1a expression in epidermal Langerhans cells: evidence from human CD1A genome-transgenic mice. J. Invest. Dermatol. 2012; 132:241–244. [PubMed: 21900947]
37. Riol-Blanco L, et al. Nociceptive sensory neurons drive interleukin-23-mediated psoriasiform skin inflammation. Nature. 2014; 510:157–161. [PubMed: 24759321]
38. Stoitzner P, Romani N, McLellan AD, Tripp CH, Ebner S. Isolation of skin dendritic cells from mouse and man. Methods Mol. Biol. 2010; 595:235–248. [PubMed: 19941117]
39. Winn MD, et al. Overview of the CCP4 suite and current developments. Acta Crystallogr. D Biol. Crystallogr. 2011; 67:235–242. [PubMed: 21460441]
40. Bricogne, G., et al. BUSTER. version 2.10.0. Global Phasing Ltd; Cambridge, UK: 2011.
41. Emsley P, Lohkamp B, Scott WG, Cowtan K. Features and development of Coot. Acta Crystallogr. D Biol. Crystallogr. 2010; 66:486–501.
42. Alshehry ZH, et al. An Efficient Single Phase Method for the Extraction of Plasma Lipids. Metabolites. 2015; 5:389–403. [PubMed: 26090945]
43. Schittenhelm RB, Sian TC, Wilmann PG, Dudek NL, Purcell AW. Revisiting the arthritogenic peptide theory: quantitative not qualitative changes in the peptide repertoire of HLA-B27 allotypes. Arthritis Rheumatol. 2015; 67:702–713. [PubMed: 25418920]

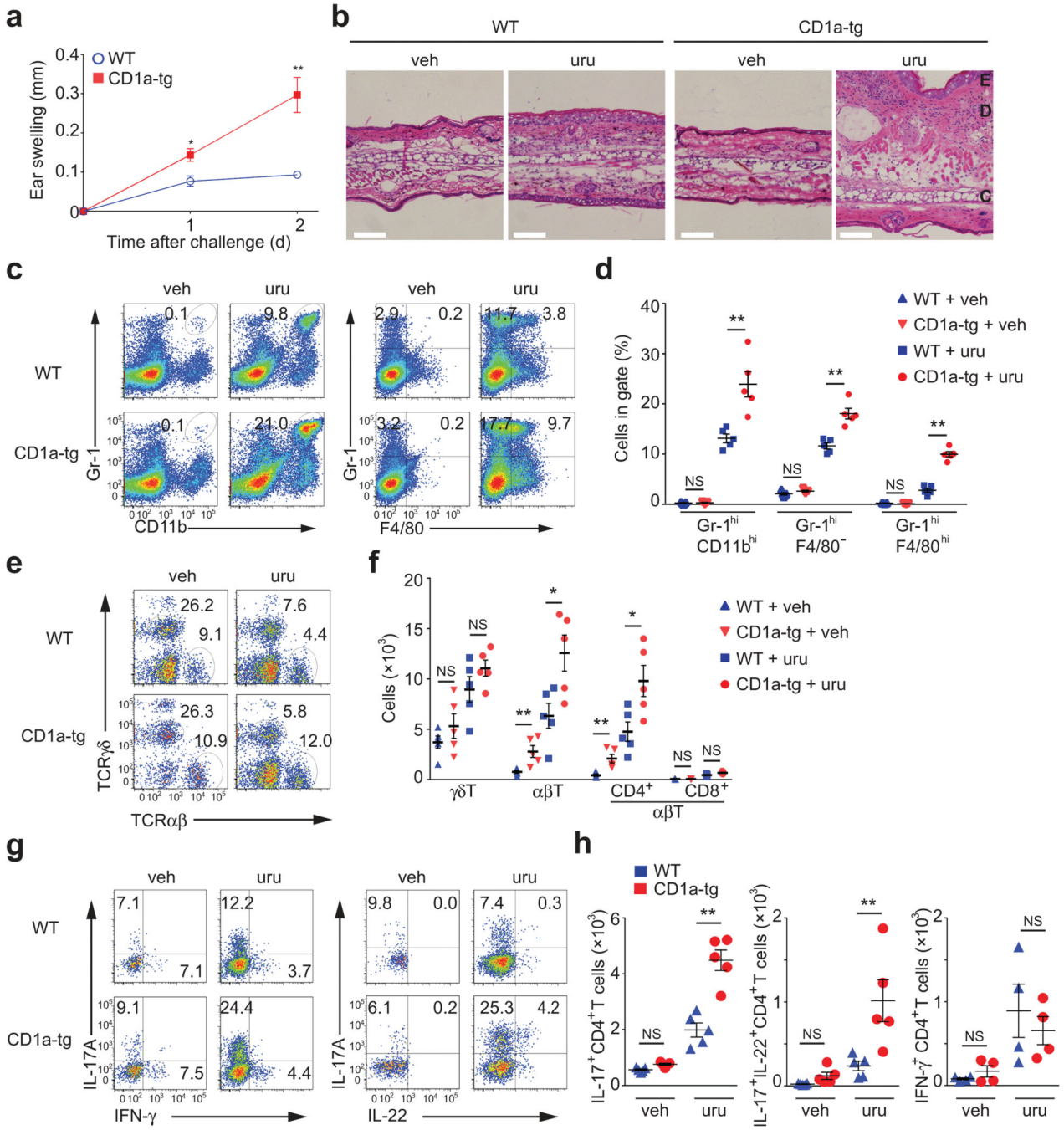

Figure 1.

CD1a facilitates T_H17-mediated skin inflammation caused by poison ivy. (**a**,**b**) Ear swelling ($n = 5$ per group) (**a**) and microscopy of hematoxylin-and-eosin-stained cross-sections of ears (**b**) in mice sensitized by painting of urushiol on the abdomen on day 0 and challenged with urushiol (uru; **a**,**b**) or vehicle (veh; **b**) on the ear on day 5, assessed on day 2 after challenge. Epidermis (E), dermis (D) and cartilage (C). Scale bar: 100 μm. (**c**-**h**) Flow cytometry analysis of granulocytes, macrophages and T cell subsets in ear skin 2 days after challenge. WT, wild-type. (**c**,**d**) Frequencies of inflammatory granulocytes ($Gr\text{-}1^{hi}CD11b^{hi}$)

and macrophages (F4/80^{+}Gr-1^{+}, or F4/80^{+}Gr-1^{-}) among all live cells. (**e**) Frequencies of αβ and γδ T cells among live CD45^{+} cells. (**f**) Absolute cell numbers of indicated T cell subsets. (**g**,**h**) Frequencies and absolute cell numbers of IFN-γ^{+}, IL-17A^{+}, and IL-22^{+} cells among TCRβ^{+}CD4^{+} cells. Each symbol represents an individual mouse (**d**,**f**,**h**). Data shown are the mean ± s.e.m. * $P < 0.05$, ** $P < 0.01$; NS, not significant, using unpaired *t*-test (**a**) or Mann-Whitney test (**d**,**f**,**h**). Data are from one experiment representative of five independent experiments with similar results.

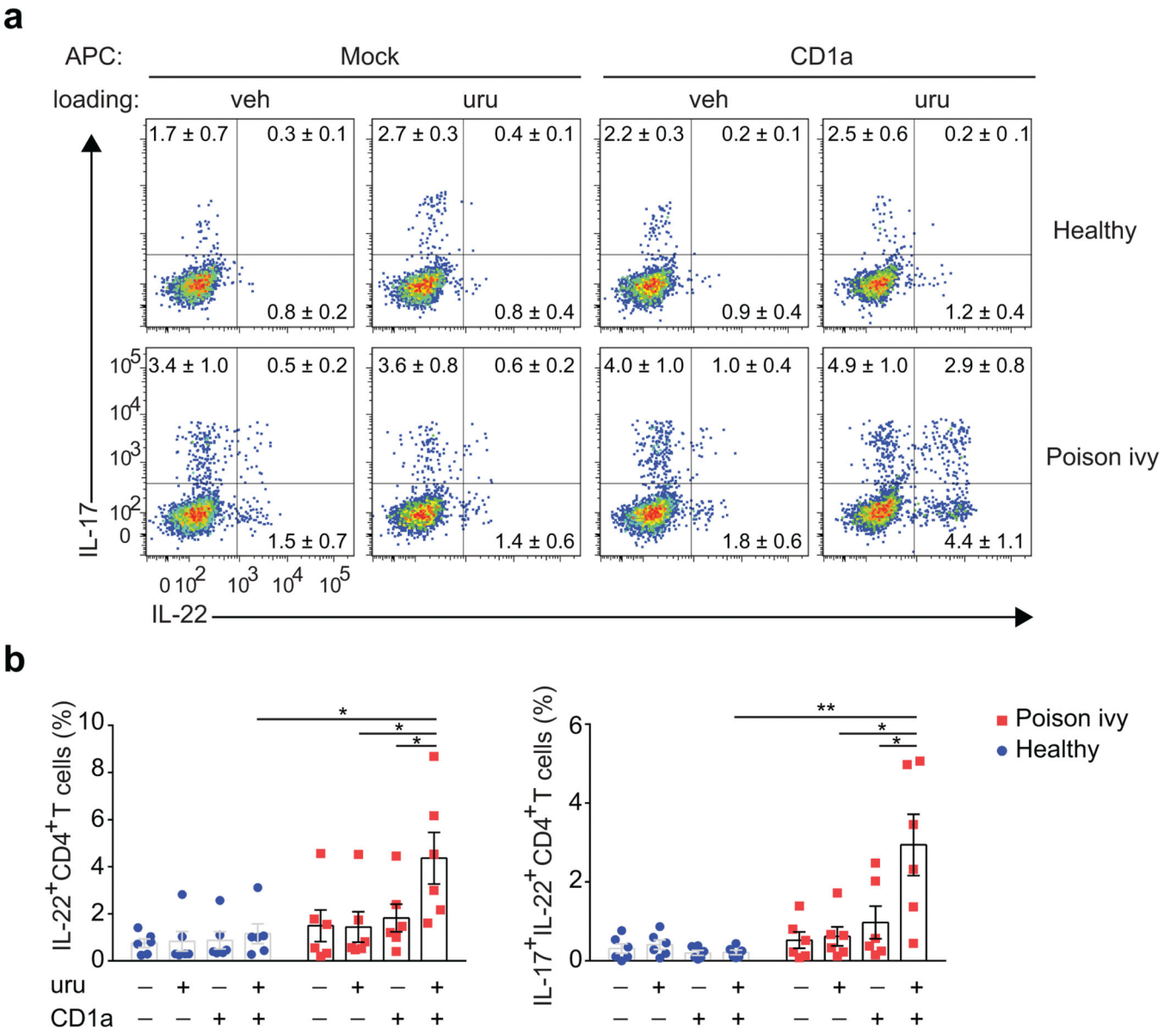

Figure 2.

Human subjects with poison ivy dermatitis show urushiol-specific T cell responses mediated by CD1a. (**a**,**b**) Flow cytometry analysis of CD45RO$^+$ memory T cells sorted from the peripheral blood of donors ($n = 6$) who experienced contact dermatitis caused by poison ivy within the last 6 months or healthy control donors ($n = 6$) and cocultured with urushiol (C15:2)- or vehicle-loaded CD1a- or mock-transfected K562 cells for 3 days. (**a**) Numbers indicate frequencies of IL-17- and IL-22-producing CD4$^+$ cells among TCRβ$^+$ cells (mean ± s.e.m.). (**b**) Quantification of percentage of IL-22$^+$ and IL-17A$^+$IL-22$^+$ cells among CD4$^+$ T cells. Each symbol represents an individual subject (**b**). Data shown are the mean ± s.e.m. * $P < 0.05$, ** $P < 0.01$; NS, not significant, using Wilcoxon test.

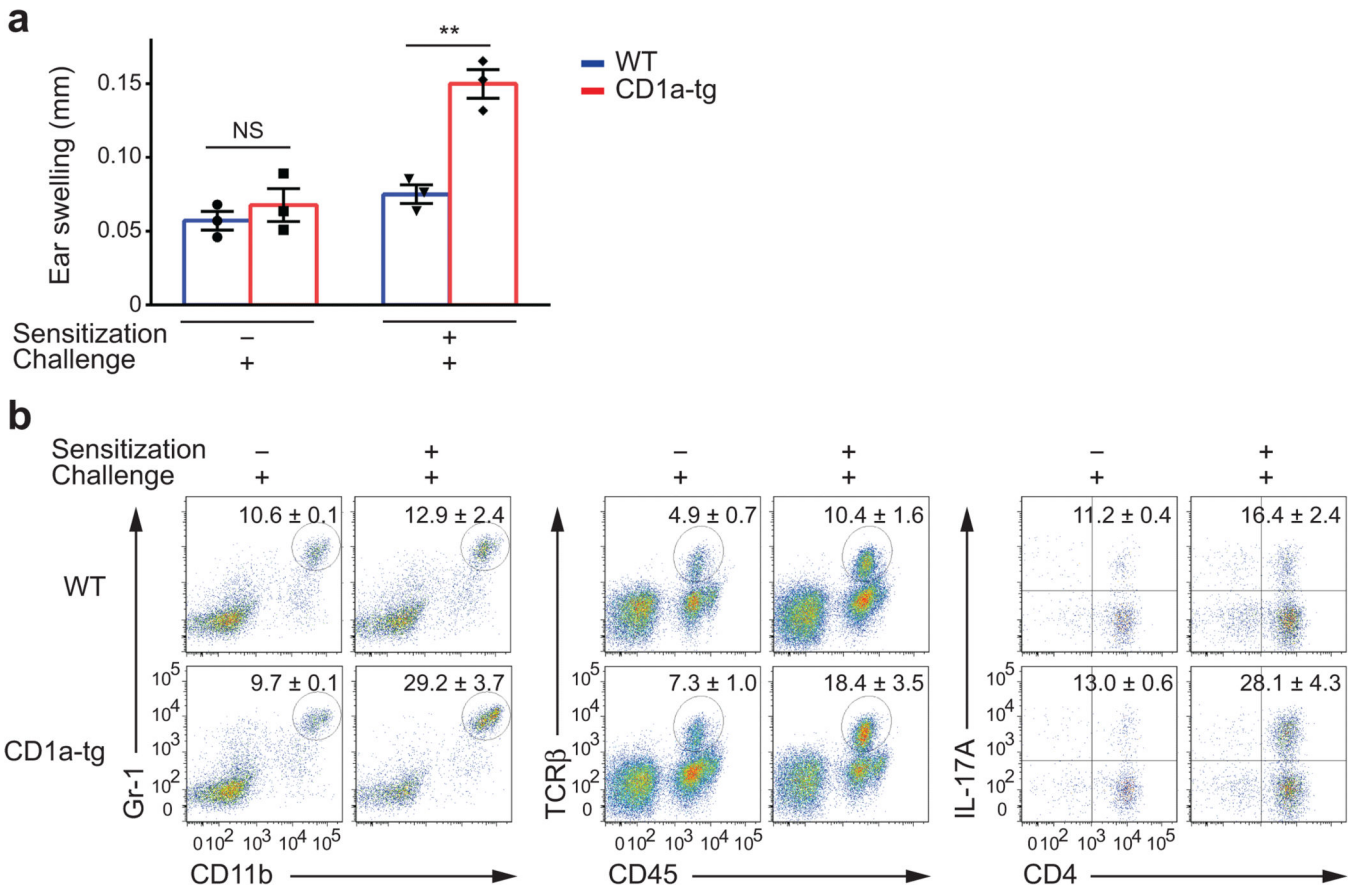

Figure 3.

Urushiol-specific T cells are primed during the sensitization phase. (**a**) Ear swelling in mice ($n = 3$ per group) with or without sensitization and challenged with urushiol on the ear on day 5, assessed on day 2 after challenge. Each symbol represents an individual mouse. (**b**) Frequencies of Gr-1^{hi}CD11b^{hi} granulocytes (left), CD45^{+}TCRβ^{+} cells among live cells (middle), and IL-17A^{+}CD4^{+} cells among TCRβ^{+} cells (right) in ears of mice ($n = 3$ per group) treated as in **a**. Numbers adjacent to outlined areas indicate percent cells (mean ± s.e.m.) in each, among the parent population. ** $P < 0.01$; NS, not significant, using unpaired *t*-test. Data are from one experiment representative of three independent experiments with similar results (**a**,**b**).

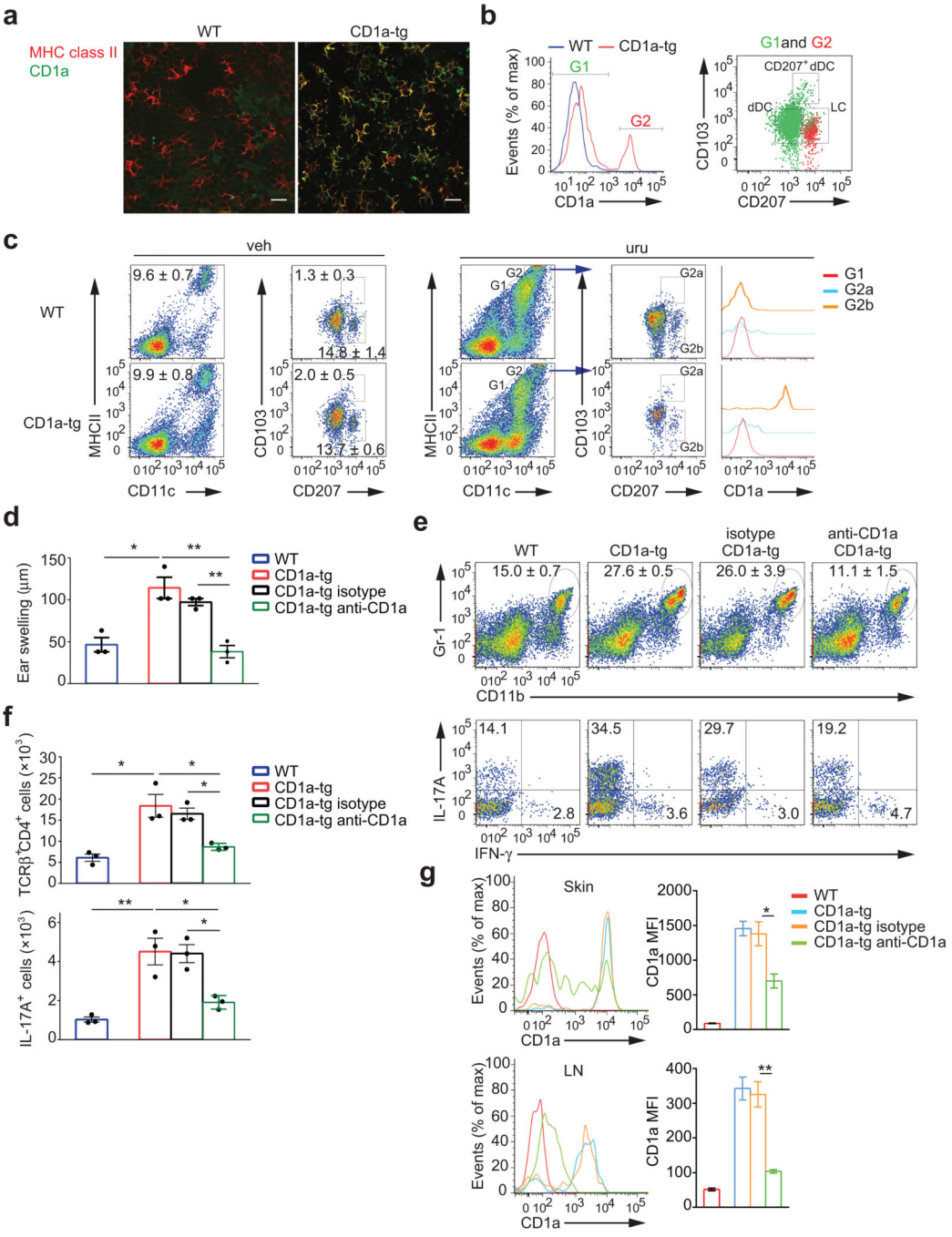

Figure 4.

CD1a expression on Langerhans cells is essential for generation of T_H17 cells and dermatitis. (**a**) Confocal microscopy of epidermal sheets stained for MHC class II and CD1a. Scale bar: 20 μm. (**b**) Flow cytometry of CD1a expression on $CD11c^+MHCII^{hi}$ cells (left panel), CD103 and CD207 (Langerin) expression in CD1a-negative (I, green dots) and CD1a-positive (II, red dots) populations of CD1a-tg mice gated from the left plot (right panel). (**c**) Flow cytometry of Langerhans cells population in ear cells isolated from mice (*n* = 3 per group) sensitized to urushiol on day 0 and challenged with vehicle (veh) or urushiol

(uru) on day 5, assessed on day 2 after challenge. CD1a expression on $CD11c^{+}MHCII^{int}$ (Gate, G1), $CD103^{+}CD207^{+}$ (G2a), and $CD103^{-}CD207^{+}$ (G2b) cells among $CD11c^{+}MHCII^{hi}$ (G2) cells of urushiol-challenged mice was further analyzed (far right). (**d-g**) Ear swelling (**d**), frequencies of $Gr\text{-}1^{hi}CD11b^{hi}$ granulocytes (**e**, top), IL-$17A^{+}$ or IFN-γ^{+} cells among $CD45^{+}TCR\gamma^{+}CD4^{+}$cells (**e**, bottom), absolute cell numbers of $CD4^{+}$ T cells (**f**, top), IL-17A-producing $CD4^{+}$ T cells (**f**, bottom), and CD1a expression on LCs in ear skin (**g**, top) and dLN (**g**, bottom) from urushiol-challenged wild-type, CD1a-tg, or CD1a-tg mice injected with anti-CD1a or isotype ($n = 3$ per group). MFI indicate mean fluorescent intensity. Each symbol represents an individual mouse (**d**,**f**). Data shown are the mean ± s.e.m. * $P < 0.05$, ** $P < 0.01$; NS, not significant, using one-way ANOVA and multiple comparisons. Data are representative of four independent experiments with similar results.

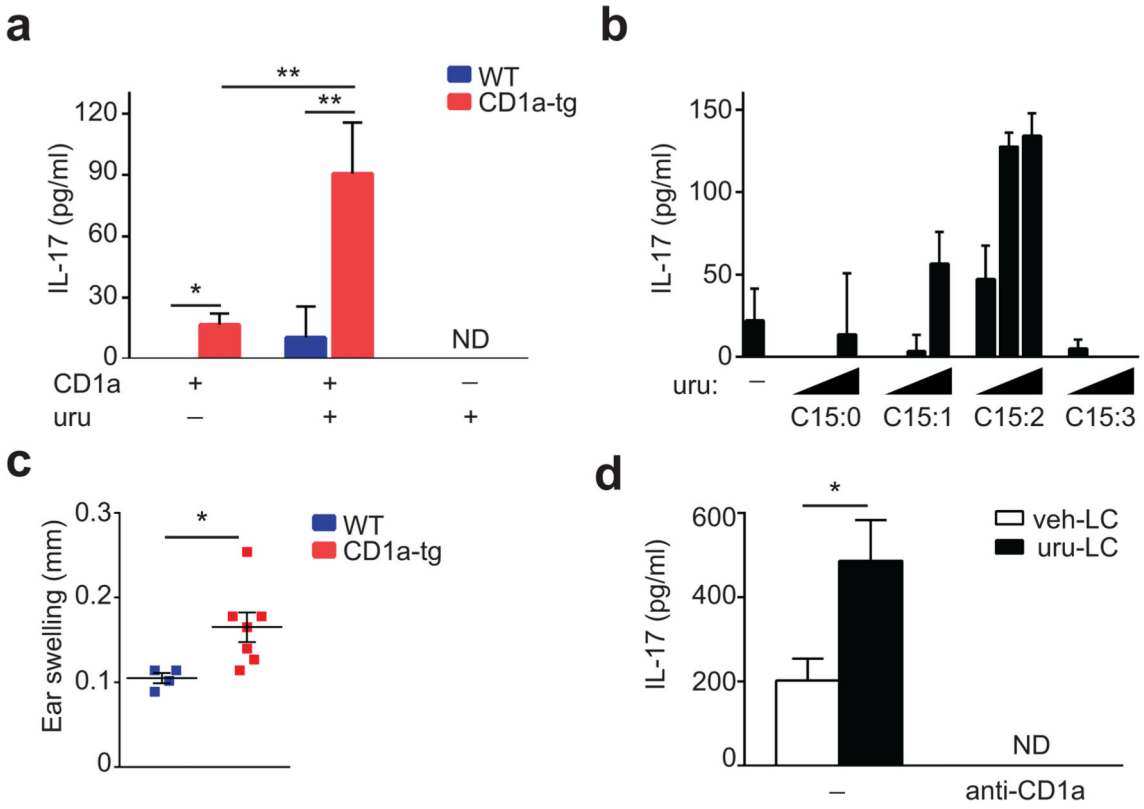

Figure 5.

Urushiol is an antigen for CD1a-restricted T cells. (**a**,**b**) Concentration of IL-17A in supernatants from skin $CD4^+$ T cells ($n = 3$) isolated on day 2 after urushiol challenge and stimulated by plate-bound CD1a loaded with natural urushiol (**a**), or various concentrations of synthetic urushiol C15:0, C15:1, C15:2, or C15:3 (**b**). (**c**) Ear swelling in wild-type ($n = 4$) and CD1a-tg mice ($n = 7$) sensitized and challenged with C15:2 urushiol, assessed on day 2 after challenge. (**d**) Concentration of IL-17A in supernatants from dLN $CD4^+$ T cells ($n = 4$) isolated from CD1a-tg mice challenged with urushiol and cocultured with skin langerhans cells (LC) pulsed with C15:2 urushiol in the presence or absence of anti-CD1a antibody; ND, not detectable. Each symbol represents an individual mouse (**c**). Data shown are the mean ± s.e.m. * $P < 0.05$, ** $P < 0.01$; NS, not significant, using unpaired *t*-test. Data are representative of five (**a**), three (**b**), four (**c**), or two (**d**) independent experiments.

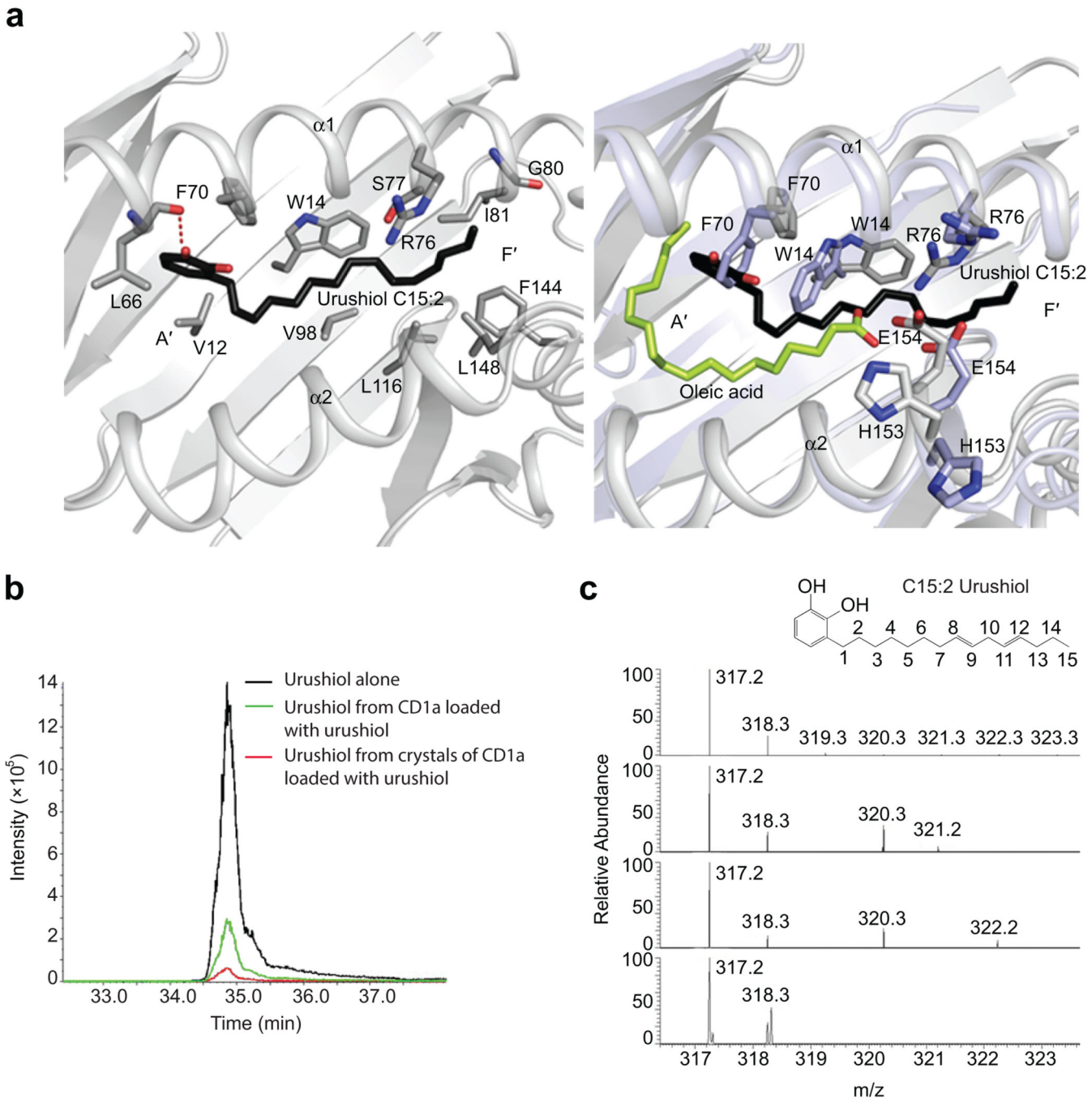

Figure 6.

CD1a binds and displays urushiol (C15:2) in its antigen-binding cleft. (**a**) Molecular interactions of urushiol (C15:2) with CD1a. Superposition of the CD1a-urushiol binary complex (in grey) and the complex of TCR-CD1a-endogenous lipid (in light blue) (PDB code: 5J1A, 4X6D). (**b**) Extracted ion chromatograms (Q1-Q3 transition) of urushiol C15:2 synthetic standard (in black), purified recombinant CD1a loaded with urushiol (in green), and crystal of CD1a-urushiol C15:2 (in red). (**c**) Accurate mass spectra for urushiol extracts comparing predicted molecular weight and isotope distribution pattern. urushiol C15:2

theoretical mass (**c**, top), urushiol C15:2 synthetic standard (**c**, upper middle), purified CD1a-urushiol C15:2 soluble extract (**c**, lower middle), and CD1a-urushiol C15:2 binary complex crystal (**c**, bottom).

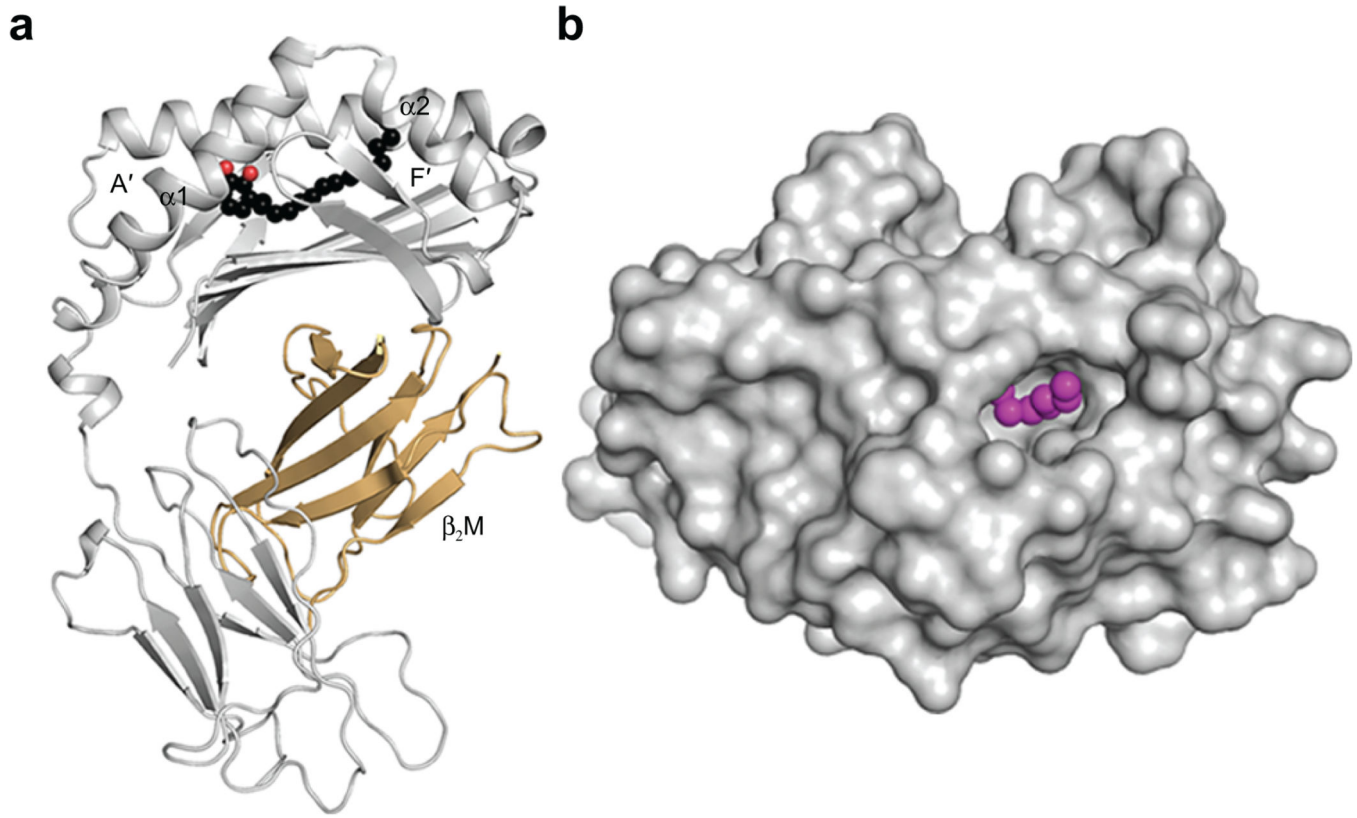

Figure 7.

Crystal structure of the CD1a-urushiol complex. (**a**) Overall cartoon representation of the binary crystal structure of CD1a-urushiol C15:2. (**b**) Top view of the molecular surface of the α1- and α2- domains of CD1a (in grey) and the bound urushiol shown as spheres (in magenta).

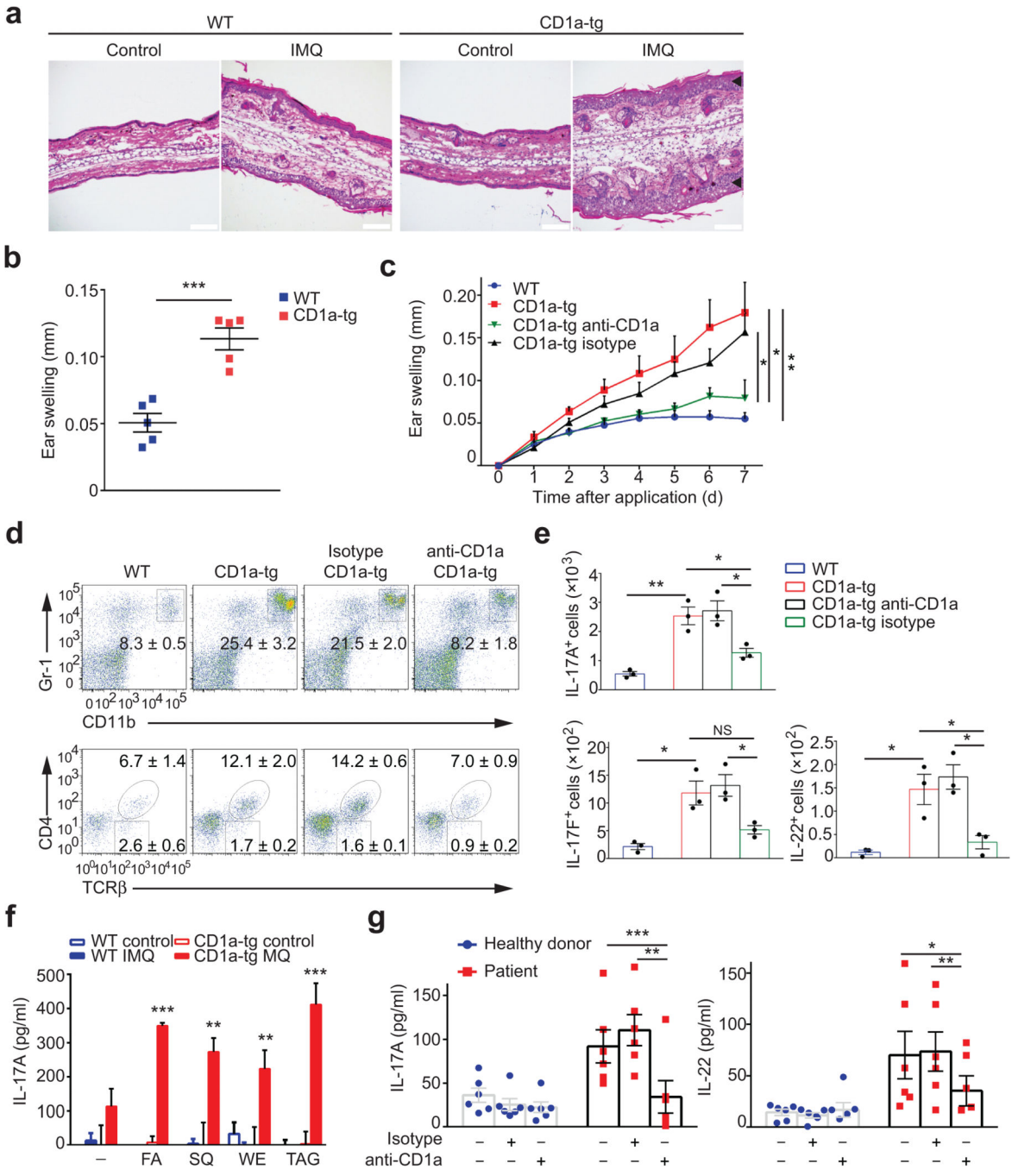

Figure 8.

CD1a is a novel target for treatment of psoriatic inflammation. (**a**) Microscopy of hematoxylin and eosin stained cross-sections of ears applied with Imiquimod (IMQ) for 6 days. Black arrows indicate epidermal thickening. Scale bar: 100 μm. (**b**) Ear swelling in mice ($n = 5$ per group) treated as in **a**. (**c**) Ear swelling of IMQ-treated wild-type ($n = 8$), CD1a-tg ($n = 8$), or CD1a-tg mice injected with anti-CD1a ($n = 8$) or isotype ($n = 6$). (**d-e**) Frequencies of Gr-1^{hi}CD11b^{hi} granulocytes and TCR-β^{+}CD4^{+} cells among live CD45^{+} cells (**d**), and absolute cell numbers of IL-17A-, IL-17F-, and IL-22-producing CD4^{+} T cells (**e**)

in ear skins of mice treated as in **c** (n = 3 per group). (**f**) Concentration of IL-17A in supernatants from dLN $CD4^+$ T cells (n = 3) isolated from mice treated or non-treated with IMQ, and stimulated by plate-bound CD1a loaded with fatty acid (FA), squalene (SQ), wax ester (WE), or triacylglycerol (TAG). (**g**) Concentration of IL-17A and IL-22 in supernatants from $CD45RO^+$ memory T cells isolated from patients with active psoriasis (n = 6), or healthy donors (n = 6), and cocultured with autologous monocyte-derived DCs in the presence of anti-CD1a or isotype. Each symbol represents an individual subject (**b**,**e**,**g**). Data shown are the mean ± s.e.m. * P<0.05, ** P<0.01, *** P<0.001, **** P<0.0001, using unpaired t-test (**b,f**), two-way ANOVA (**c**), and one-way ANOVA (**e,g**). Data are representative of five (**b**), or three independent experiments (**c-f**).